

Supplemental Information for:
Probing the local structures and protonic conduction pathways
in scandium substituted BaZrO₃
by multinuclear solid-state NMR spectroscopy

Lucienne Buannic,¹ Frédéric Blanc,¹ Ivan Hung,²

Zhehong Gan² and Clare Grey^{1,3*}

¹ Department of Chemistry,

SUNY Stony Brook,

Stony Brook, NY 11790-3400, USA,

² National High Magnetic Field Laboratory

1800 E. Paul Dirac Drive,

Tallahassee, FL 32310 – 3706, USA.

³ Department of Chemistry,

University of Cambridge, Lensfield Road,

Cambridge, CB2 1EW, UK.

* Email: cgrey@notes.cc.sunysb.edu.

Experimental

To confirm the simulation parameters extracted from the static ^{45}Sc spectra of the dry samples at 8.5 T, additional experiments were run at 11.7 T. Static ^{45}Sc NMR experiments were performed on a 11.7 T wide bore using a single channel 4 mm probe tuned to 121.44 MHz. Quadrupolar echo experiments were recorded using a selective $\pi/2 = 0.5 \mu\text{s}$ at a rf field amplitude of 125 kHz with an evolution period of 20 μs and a recycle delay of 1.5 s.

Results and discussion

The static ^{45}Sc spectra of the dry samples at 11.7 T are gathered in Figure S1. As expected for this field, the width of the quadrupolar signal reduces as the second quadrupolar coupling effect decreases at higher field. However the parameters used to fit the spectra at 8.5 T simulate very well the spectra at 11.7 T (Table 1) providing additional support for these fits. The satellite transitions for the 6 coordinated scandium site are less pronounced at higher field rendering the evaluation of the asymmetry parameter η_Q more difficult.

The ^{45}Sc spectra of the hydrated samples obtained at 8.5T are more difficult to simulate (Figures S2, S3 and S4). $\text{BaZr}_{0.95}\text{Sc}_{0.05}\text{O}_{2.975}(\text{OH})_{0.01}$ can be reasonably well simulated by either assuming that there is one site with a C_Q of 0.4MHz, or two sites with C_Q of 1.1 and 18MHz, the site with the smaller C_Q presumably corresponding to the six-coordinated scandium cations. In this model, the site with the larger C_Q corresponds to a defect site, possibly corresponding to a residual 5-coordinated site, or more likely, based on the chemical shift, a distorted 6 coordinate environment which could be generated by filling the oxygen vacancy in the 5 coordinate environment ($\text{ScO}_5\square$) with an OH defect. The MQMAS data supports the presence of a second distorted 6-coordinate site. The spectra of both $\text{BaZr}_{0.85}\text{Sc}_{0.15}\text{O}_{2.925}(\text{OH})_{0.10}$ and $\text{BaZr}_{0.70}\text{Sc}_{0.30}\text{O}_{2.85}(\text{OH})_{0.20}$ are dominated by resonances due a six-coordinated scandium environments with a C_Q of approximately 1.5 MHz (as determined

by simulation (Figures S3, S4)). They also appear to contain contributions from a number of broader resonances, which reflect a distribution in local environments, making the spectra non-trivial to fit. Further analysis of the static spectra to account for distributions in NMR parameters is beyond the scope of this work.

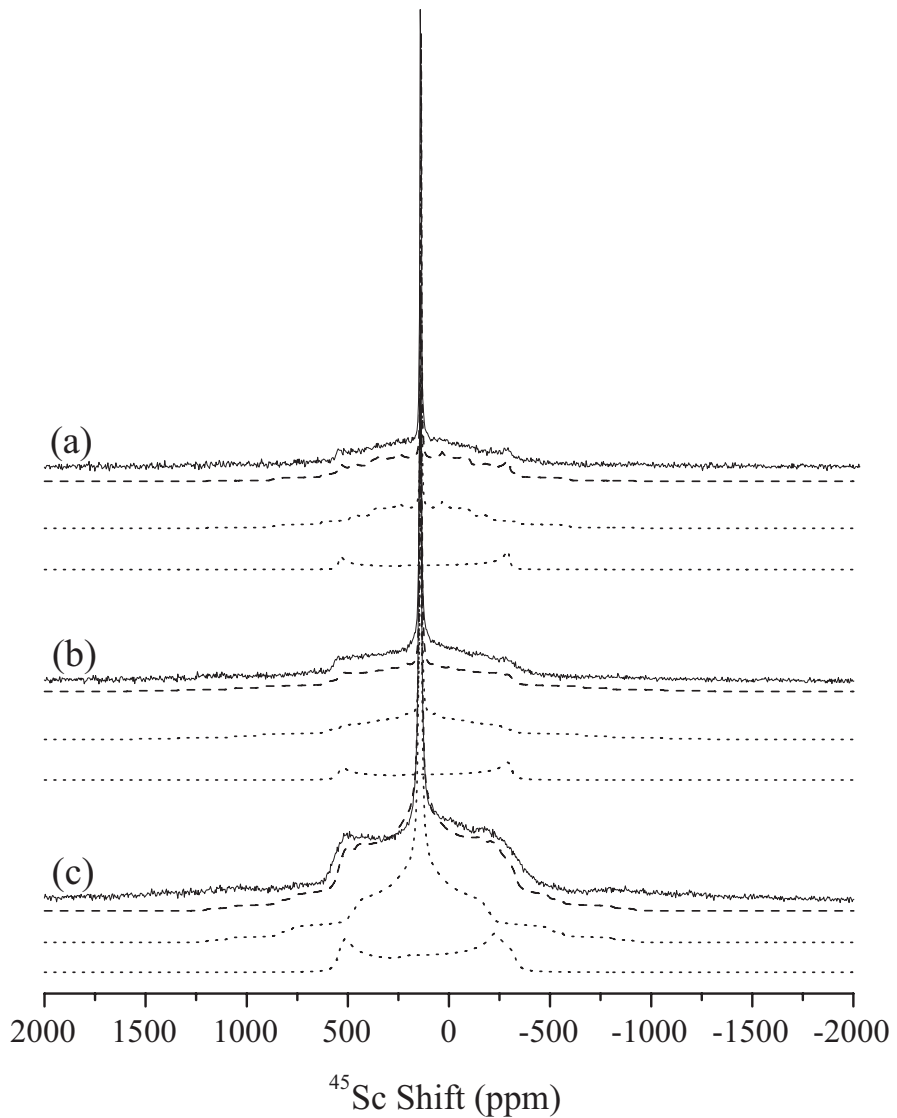


Figure S1. Static ^{45}Sc quadrupolar echo spectra of $\text{BaZr}_{1-x}\text{Sc}_x\text{O}_{3-x/2}$ obtained at 11.7 T with a relaxation delay of 1.5 s. (a) $\text{BaZr}_{0.95}\text{Sc}_{0.05}\text{O}_{2.985}$ (6104 transients). (b) $\text{BaZr}_{0.85}\text{Sc}_{0.15}\text{O}_{2.925}$ (4512 transients). (c) $\text{BaZr}_{0.70}\text{Sc}_{0.30}\text{O}_{2.85}$ (6224 transients). Simulations performed with the parameters reported in Table 1, are shown below the spectra of the dry samples. The dotted lines represent the two individual components used to simulate each spectrum and the dashed lines are the sum of the two components.

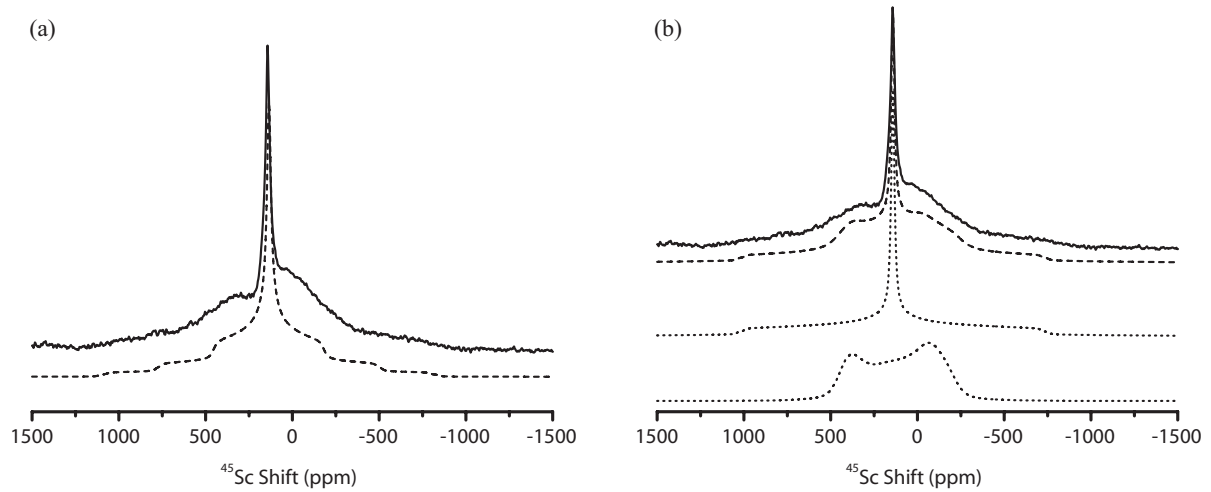


Figure S2. Experiment and simulations of the static ^{45}Sc spectrum of $\text{BaZr}_{0.95}\text{Sc}_{0.05}\text{O}_{2.985}(\text{OH})_{0.01}$ obtained at 8.5 T. Simulation with (a) one site only with $\delta_{\text{iso}} = 142(2)$ ppm, $C_Q = 0.4(2)$ and $\eta_Q = 0.9(1)$, (b) two sites with $\delta_{\text{iso}} = 142(2)$ ppm, $C_Q = 1.1(1)$ and $\eta_Q = 0.9(1)$ for the first site and $\delta_{\text{iso}} = 180(20)$ ppm, $C_Q = 18(2)$ and $\eta_Q = 0.2(1)$ for the second site.

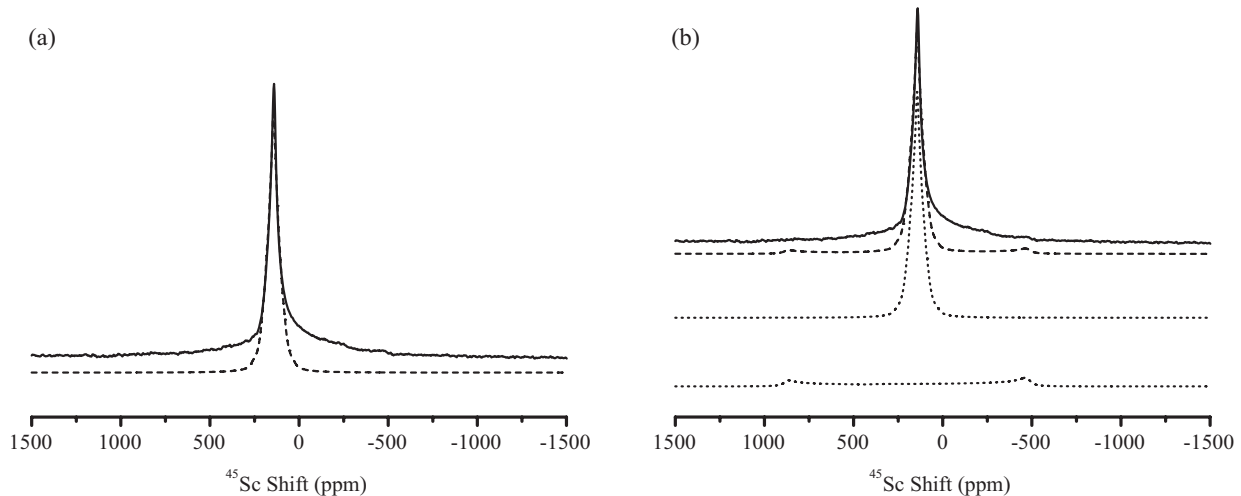


Figure S3. Experiment and simulations of the static ^{45}Sc spectrum of $\text{BaZr}_{0.85}\text{Sc}_{0.15}\text{O}_{2.925}(\text{OH})_{0.10}$ obtained at 8.5 T. Simulation with (a) one site only with $\delta_{\text{iso}} = 144(2)$ ppm and $C_Q \leq 1.5$; η_Q cannot be determined since the lineshape is not distinct, (b) two sites with $\delta_{\text{iso}} = 144(2)$ ppm and $C_Q \leq 1.5$; η_Q cannot be determined for the first site and $\delta_{\text{iso}} \approx 310(70)$ ppm, $C_Q = 28(3)$ and $\eta_Q = 0.0(1)$ for the second site. Both simulations fail to capture further broad components, which indicate that additional distorted sites are present.

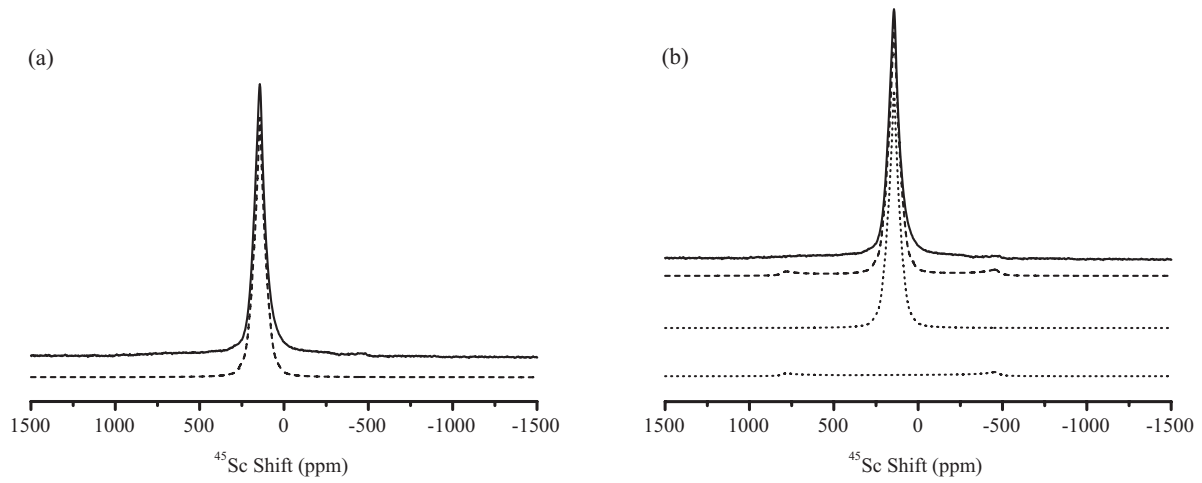


Figure S4. Experiment and simulation of the static ^{45}Sc spectrum of $\text{BaZr}_{0.70}\text{Sc}_{0.30}\text{O}_{2.85}(\text{OH})_{0.20}$ obtained at 8.5 T. Simulation with (a) one site only with $\delta_{\text{iso}} = 144(2)$ ppm, $C_Q \leq 1.5$ and η_Q is undetermined due to the lack of lineshape, (b) two sites with $\delta_{\text{iso}} = 144(2)$ ppm, $C_Q = 1.5(8)$ and η_Q is undertermined for the first site and $\delta_{\text{iso}} \approx 290(50)$ ppm, $C_Q = 27(3)$ and $\eta_Q = 0.0(1)$ for the second site.

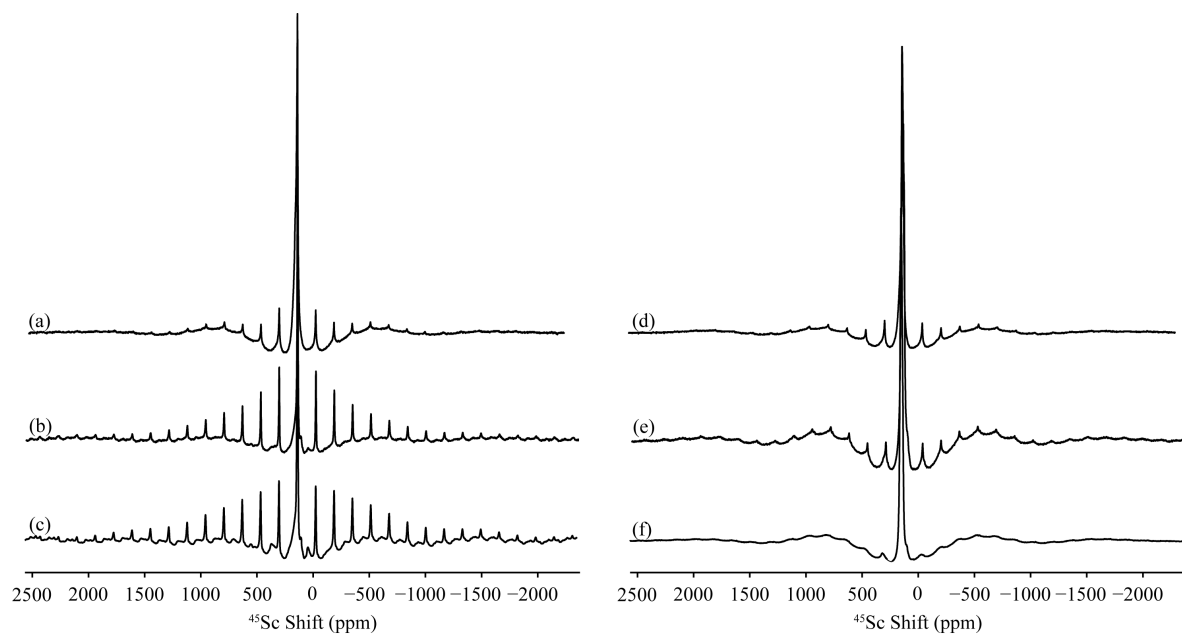


Figure S5. Full width of the ^{45}Sc MAS NMR single pulse spectra of $\text{BaZr}_{1-x}\text{Sc}_x\text{O}_{3-x/2}$ and $\text{BaZr}_{1-x}\text{Sc}_x\text{O}_{3-x/2}(\text{OH})_y$ obtained at 19.6 T. (a) $\text{BaZr}_{0.95}\text{Sc}_{0.05}\text{O}_{2.985}$. (b) $\text{BaZr}_{0.85}\text{Sc}_{0.15}\text{O}_{2.925}$. (c) $\text{BaZr}_{0.70}\text{Sc}_{0.30}\text{O}_{2.85}$. (d) $\text{BaZr}_{0.95}\text{Sc}_{0.05}\text{O}_{2.975}(\text{OH})_{0.01}$. (e) $\text{BaZr}_{0.85}\text{Sc}_{0.15}\text{O}_{2.925}(\text{OH})_{0.10}$. (f) $\text{BaZr}_{0.70}\text{Sc}_{0.30}\text{O}_{2.85}(\text{OH})_{0.20}$. 2048 transients were collected for all spectra.

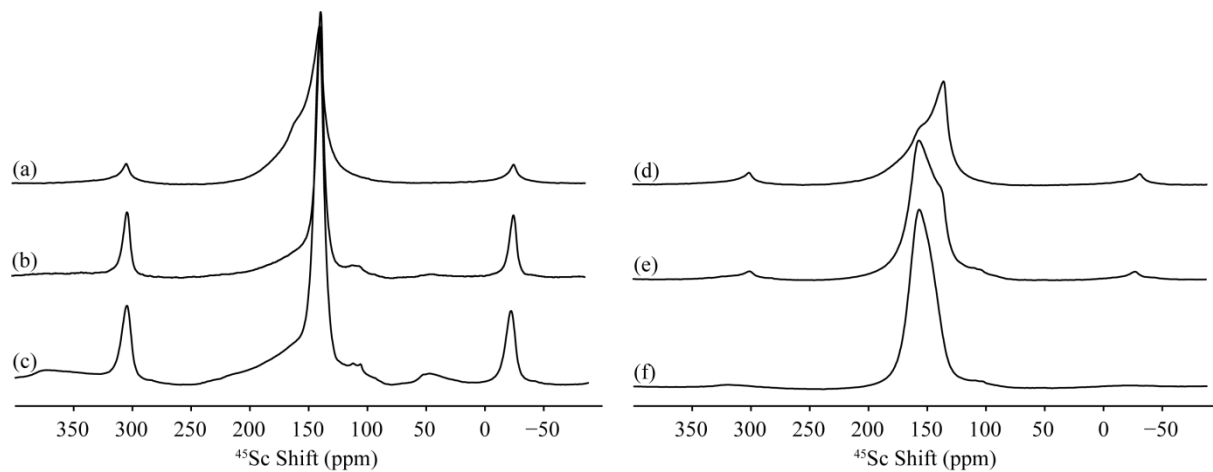


Figure S6. Zoom in the 400 to -100 ppm region of the ^{45}Sc MAS NMR single pulse spectra of $\text{BaZr}_{1-x}\text{Sc}_x\text{O}_{3-x/2}$ and $\text{BaZr}_{1-x}\text{Sc}_x\text{O}_{3-x/2}(\text{OH})_y$ obtained at 19.6 T. (a) $\text{BaZr}_{0.95}\text{Sc}_{0.05}\text{O}_{2.985}$. (b) $\text{BaZr}_{0.85}\text{Sc}_{0.15}\text{O}_{2.925}$. (c) $\text{BaZr}_{0.70}\text{Sc}_{0.30}\text{O}_{2.85}$. (d) $\text{BaZr}_{0.95}\text{Sc}_{0.05}\text{O}_{2.975}(\text{OH})_{0.01}$. (e) $\text{BaZr}_{0.85}\text{Sc}_{0.15}\text{O}_{2.925}(\text{OH})_{0.10}$. (f) $\text{BaZr}_{0.70}\text{Sc}_{0.30}\text{O}_{2.85}(\text{OH})_{0.20}$. 2048 transients were collected for all spectra.

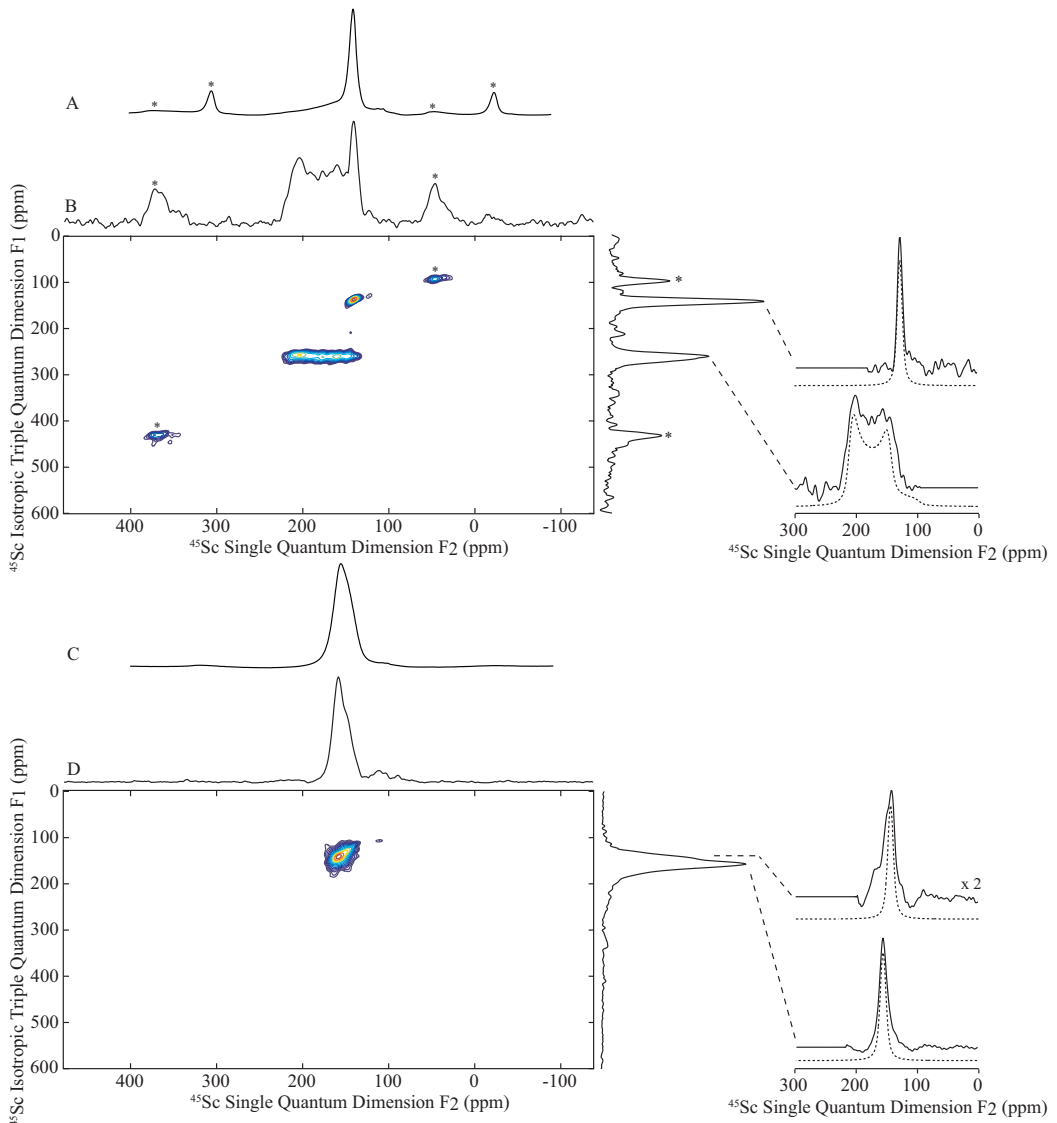


Figure S7. ^{45}Sc MAS NMR single pulse spectra of $\text{BaZr}_{0.70}\text{Sc}_{0.30}\text{O}_{2.85}$ (A) and $\text{BaZr}_{0.70}\text{Sc}_{0.30}\text{O}_{2.85}(\text{OH})_{0.20}$ (C) and two-dimensional sheared triple-quantum ^{45}Sc MAS spectrum of (B) $\text{BaZr}_{0.70}\text{Sc}_{0.30}\text{O}_{2.85}$ and (D) $\text{BaZr}_{0.70}\text{Sc}_{0.30}\text{O}_{2.85}(\text{OH})_{0.20}$ obtained at 19.6 T.

For (A), 960 transients were accumulated for each of 12 t_1 increment at a recycle rate of 0.4 s while for (B) 9600 transients were accumulated for each of 16 t_1 increment at a recycle rate of 0.5 s. Top: Anisotropic skyline projection. The asterix denotes the spinning side bands. Right: Isotropic skyline projection of the 2D 3Q MAS. Cross sections (full lines) extracted parallel to F_2 of the 2D 3Q MAS spectrum at: (A) δ_1 of 143 (top) and 266 (bottom) ppm along with the best fit simulation (dashed lines) using the parameters given in Table 1 and Table S2.

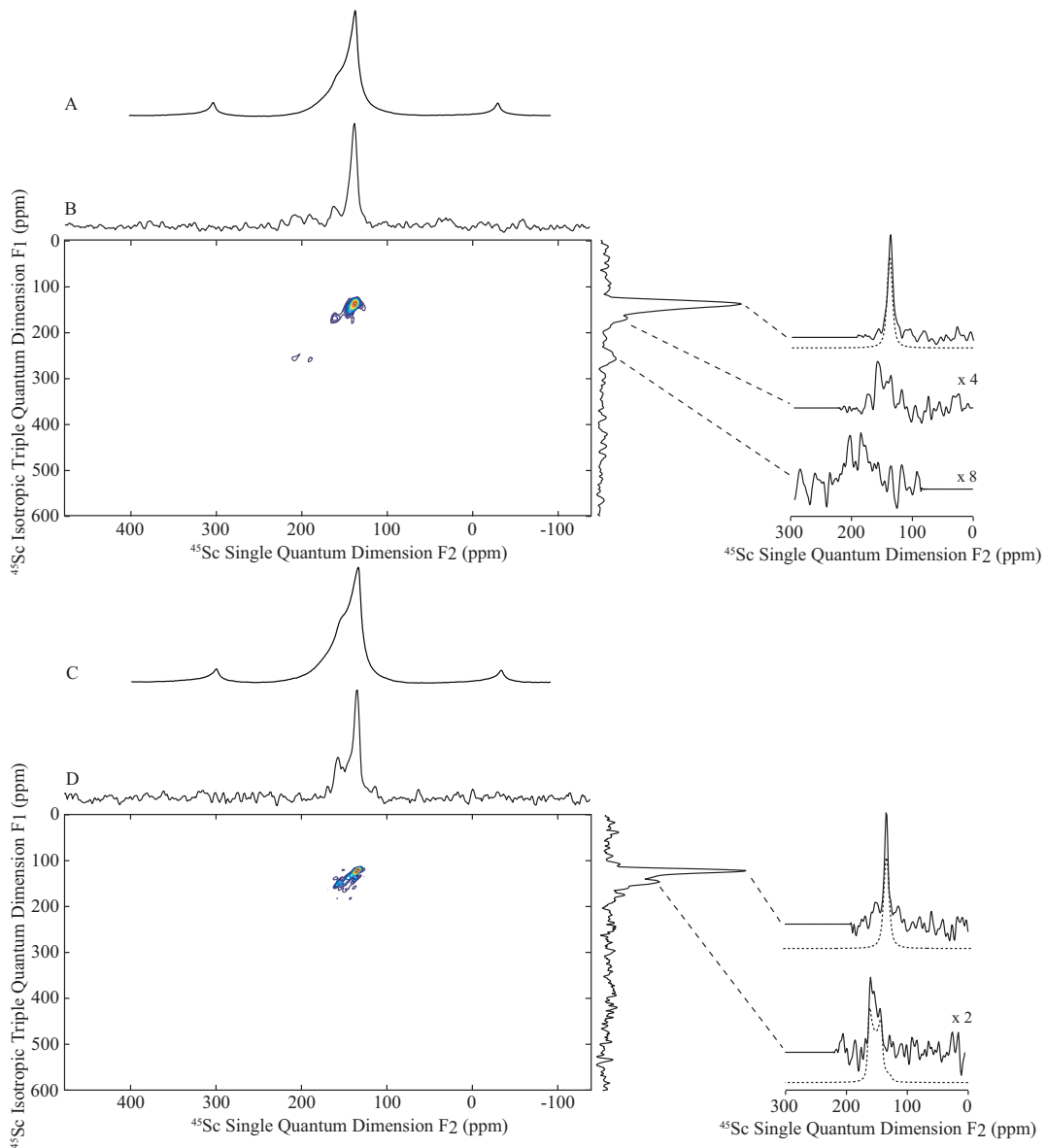


Figure S8. ^{45}Sc MAS NMR single pulse spectra of $\text{BaZr}_{0.95}\text{Sc}_{0.05}\text{O}_{2.975}$ (A) and $\text{BaZr}_{0.95}\text{Sc}_{0.05}\text{O}_{2.975}(\text{OH})_{0.01}$ (C) and two-dimensional sheared triple-quantum ^{45}Sc MAS spectrum of (B) $\text{BaZr}_{0.95}\text{Sc}_{0.05}\text{O}_{2.975}$ and (D) $\text{BaZr}_{0.95}\text{Sc}_{0.05}\text{O}_{2.975}(\text{OH})_{0.01}$ obtained at 19.6 T. 24000 transients were accumulated for each of 12 (for A) and 16 (for B) t_1 increment at a recycle rate of 0.5 s. Top: Anisotropic skyline projection. Right: Isotropic skyline projection of the 2D 3Q MAS. Cross sections (full lines) extracted parallel to F₂ of the 2D 3Q MAS spectrum at: (A) δ_1 of 139 (top), 170 (middle) and 257 (bottom) ppm along with the best fit simulation (dashed lines) using the parameters given in Table 1 and Table S2.

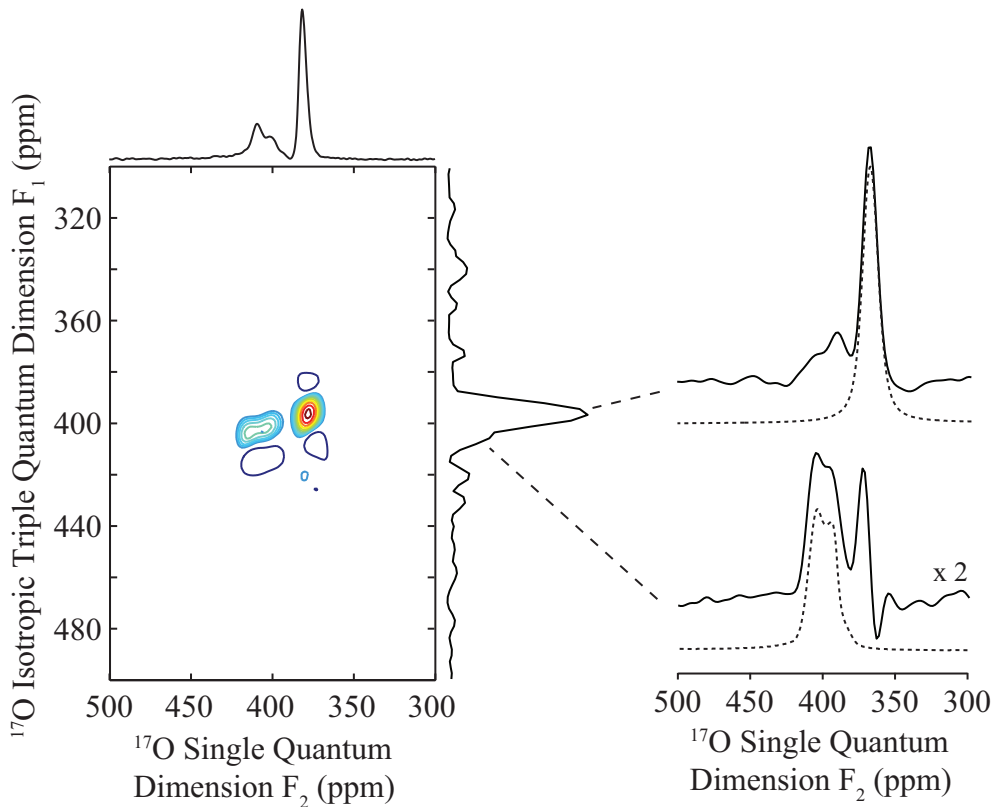


Figure S9. Two-dimensional sheared triple-quantum ^{17}O MAS spectrum of $\text{BaZr}_{0.85}\text{Sc}_{0.15}\text{O}_{2.925}$ obtained at 14.1 T. 792 transients were accumulated for each of 16 t_1 increment. Top: NMR Spectrum. Right: Isotropic projection of the 2D 3Q MAS. Cross sections (full lines) extracted parallel to F_2 of the 2D 3Q MAS spectrum at δ_1 of 396 (top) and 403 (bottom) ppm along with the best fit simulation (dashed lines) using the parameters in Tables 3 and S3.

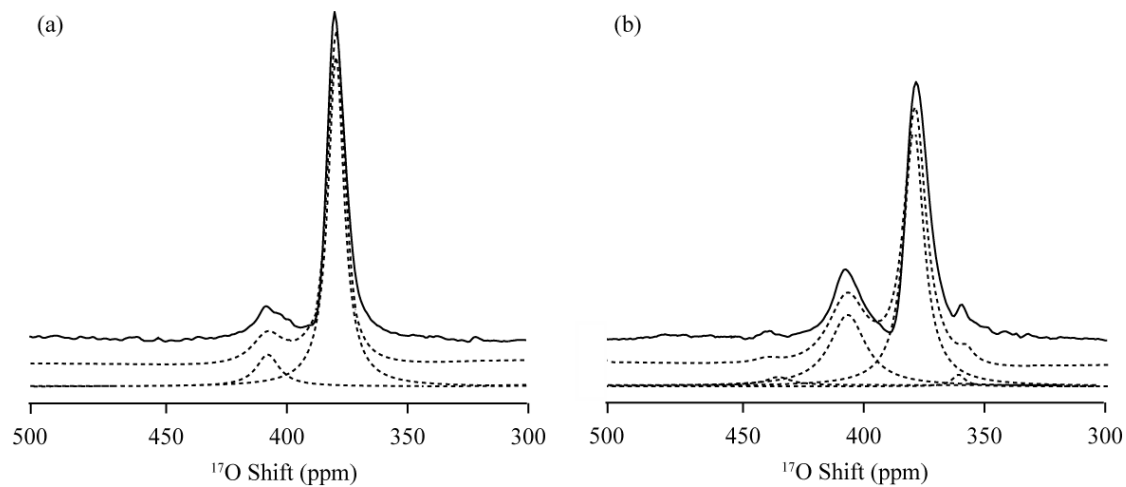


Figure S10. ^{17}O MAS NMR spectra of $\text{BaZr}_{1-x}\text{Sc}_x\text{O}_{3-x/2}$ obtained at 21.1 T. (a) $\text{BaZr}_{0.85}\text{Sc}_{0.15}\text{O}_{2.925}$. (b) $\text{BaZr}_{0.70}\text{Sc}_{0.30}\text{O}_{2.85}$. Spectral deconvolution and simulation (dashed lines) are shown as a semi quantitative analysis. A zoom of the ^{17}O central transition of the spectra is only shown.

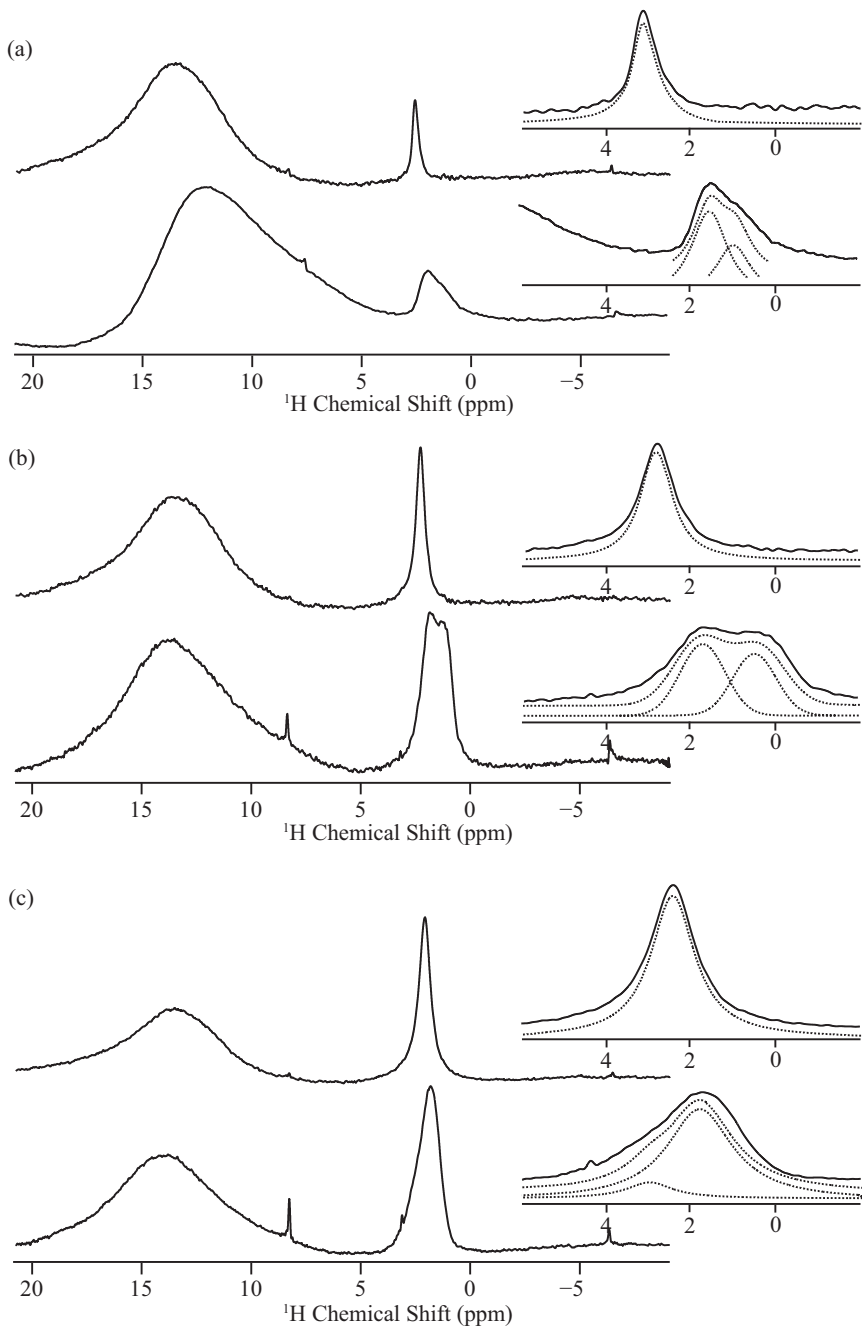


Figure S11. Variable Temperature High Resolution ^1H MAS NMR spectra of $\text{BaZr}_{1-\text{x}}\text{Sc}_{\text{x}}\text{O}_{3-\text{x}/2}(\text{OH})_{\text{y}}$. (a) $\text{BaZr}_{0.95}\text{Sc}_{0.05}\text{O}_{2.975}(\text{OH})_{0.01}$. (b) $\text{BaZr}_{0.85}\text{Sc}_{0.15}\text{O}_{2.925}(\text{OH})_{0.10}$ and (c) $\text{BaZr}_{0.70}\text{Sc}_{0.30}\text{O}_{2.85}(\text{OH})_{0.20}$. Top: Spectra obtained at 300K. Bottom: Spectra obtained at 110 K. The spectra were recorded using windowed DUMBO-1 homonuclear decoupling scheme during acquisition as explained in the materials and methods section. The inserts show a zoom in the 6 to -2 ppm range region. The signal at around 12 ppm arises from the probe background.

Table S1. Experimental ^{45}Sc NMR parameters (Triple Quantum MAS shifts δ_1 ; Isotropic Chemical Shifts δ_{iso} ^[a]; Quadrupolar Parameter P_Q ^[b]; Isotropic Second-Order Quadrupolar Shifts δ_Q ^[c]; Quadrupolar Coupling Constants C_Q ^[d] and Quadrupolar Asymmetries η_Q ^[d]) extracted from the 3Q MQMAS spectra of $\text{BaZr}_{1-x}\text{Sc}_x\text{O}_{3-x/2}$ ($x = 0.05 - 0.30$) obtained at 19.6 T.

x	δ_1 / p.p.m.	δ_{iso} / p.p.m.	δ_Q / p.p.m.	C_Q / MHz	P_Q / MHz	η_Q	Assignments
0.05	139(1)	139(1)	1(1)	0.6(1)	0.6(2)	0.4(1)	Sc^{VI}
	170(1)	167(1)	5(1)	- ^[e]	- ^[e]	- ^[e]	$\text{Sc}^{\text{VI}} \text{ OH}$
	257(1)	240(5)	31(1)	- ^[e]	- ^[e]	- ^[e]	Sc^{V}
Hyd ^[f]	136(1)	142(2)	1(3)	1.1(1)	1.2(8)	0.9(1)	Sc^{VI}
	162(1)	160(1)	3(1)	8(1)	8(1)	0.0(3)	$\text{Sc}^{\text{VI}} \text{ OH}$
0.15	138(1)	138(2)	1(1)	0.8(2)	0.8(2)	0.5(2)	Sc^{VI}
	262(1)	235(5)	55(4)	31(1)	31(2)	0.0(1)	Sc^{V}
Hyd ^[f]	142(1)	144(2)	3(3)	1.5(4)	1.5(8)	- ^[g]	Sc^{VI}
	165(5)	162(1)	4(1)	7(1)	7(1)	0.0(3)	$\text{Sc}^{\text{VI}} \text{ OH}$
0.30	143(1)	142(1)	1(1)	0.6(2)	0.7(12)	0.8(1)	Sc^{VI}
	266(1)	240(10)	54(4)	31(2)	31(4)	0.0(1)	Sc^{V}
Hyd ^[f]	144(3)	144(2)	1(8)	1.5(8)	1.5(16)	- ^[g]	Sc^{VI}
	165(1)	162(2)	4(3)	7(1)	7(1)	0.0(3)	$\text{Sc}^{\text{VI}} \text{ OH}$

^[a] Determined as $\delta_{\text{iso}} = (10/27) \times \delta_2 + (17/27) \times \delta_1$ obtained from the δ_1 and δ_2 positions (in p.p.m.) of the centre of gravity of each two-dimensional ridge line shape. ^[b] Determined as $P_Q = C_Q \times \sqrt{1+\eta^2/3}$.

^[c] Determined as $\delta_Q = (17/27) \times (\delta_2 - \delta_1)$. ^[d] Determined from best simulation of each δ_2 cross sections. The C_Q of the Sc^{VI} corresponds to the upper limit. ^[e] Signal too weak and in the limit of detection of the MQMAS experiment to be simulated with precision. ^[f] Hydrated samples. ^[g] Not determined due to the lack of signal lineshape.